

Janus effect of inter-orbital hybridization on correlation strength of strongly correlated systems: A dynamical mean-field study

Jian Sun(孙健), Yinchang Zhao(赵银昌), and Chao Lian(廉超)

Citation: Chin. Phys. B, 2026, 35 (**2**): 027103. DOI: 10.1088/1674-1056/adf040
http://cpb.iphy.ac.cn; http://iopscience.iop.org/cpb

What follows is a list of articles you may be interested in

Interacting Dirac semi-metal state in nonsymmorphic Kondo-lattice compound $CeAgSb_2$

Da-Liang Guo(郭达良), and Huan Li(黎欢)
Chin. Phys. B, 2025, 34 (**6**): 067102. DOI: 10.1088/1674-1056/adc6f6

Quantitative determination of the critical points of Mott metal—insulator transition in strongly correlated systems

Yuekun Niu(牛月坤), Yu Ni(倪煜), Jianli Wang(王建利), Leiming Chen(陈雷鸣), Ye Xing(邢晔), Yun Song(宋筠), and Shiping Feng(冯世平)
Chin. Phys. B, 2024, 33 (**1**): 017102. DOI: 10.1088/1674-1056/ad0719

Structural, electronic and magnetic properties of Fe-doped strontium ruthenates

Nan Liu(刘楠), Xiao-Chao Wang(王晓超), and Liang Si(司良)
Chin. Phys. B, 2023, 32 (**11**): 117101. DOI: 10.1088/1674-1056/ad0112

Electronic structure of cuprate-nickelate infinite-layer heterostructure

Dachuan Chen(陈大川), Paul Worm, Liang Si(司良), Chunxiao Zhang(张春小), Fenglin Deng(邓凤麟), Peiheng Jiang(蒋沛恒), and Zhicheng Zhong(钟志诚)
Chin. Phys. B, 2023, 32 (**8**): 087105. DOI: 10.1088/1674-1056/acd368

Mott transition in ruby lattice Hubbard model

An Bao(保安)
Chin. Phys. B, 2019, 28 (**5**): 057101. DOI: 10.1088/1674-1056/28/5/057101

Janus effect of inter-orbital hybridization on correlation strength of strongly correlated systems: A dynamical mean-field study

Jian Sun(孙健)[1,†], Yinchang Zhao(赵银昌)[2], and Chao Lian(廉超)[3]

[1] *School of Mathematics, Physics, and Statistics, Shanghai Polytechnic University, Shanghai* 201209, *China*
[2] *Department of Physics, Yantai University, Yantai* 264005, *China*
[3] *Beijing National Laboratory for Condensed Matter Physics, Institute of Physics, Chinese Academy of Sciences, Beijing* 100190, *China*

(Received 31 March 2025; revised manuscript received 14 July 2025; accepted manuscript online 16 July 2025)

In multi-orbital systems, the correlation strength is typically attributed to Coulomb interactions and Hund's couplings. However, this study demonstrates that on-site inter-orbital hybridization can also significant influence the correlation strength of the system. We investigate the impact of on-site inter-orbital hybridization on the correlation strength of a two-orbital Hubbard model on a square lattice using the dynamical mean-field theory combined with Lanczos exact diagonalization. Our findings reveal a distinct Janus effect: on-site inter-orbital hybridization enhances correlation strength in the non-half-filled regime while suppresses it at half-filling. This dual role of on-site inter-orbital hybridization provides a fundamental mechanism for tuning the strength of correlations in multi-orbital systems.

Keywords: strongly correlated multi-orbital system, inter-orbital hybridization, dynamical mean-field theory

PACS: 71.27.+a, 71.30.+h, 71.10.Fd

DOI: 10.1088/1674-1056/adf040 **CSTR:** 32038.14.CPB.adf040

1. Introduction

Multi-orbital correlated electron systems have attracted significant attention in recent years. Many newly discovered materials, such as iron-based[1–5] and nickel-based[6–11] high-temperature superconductors, ruthenates like $Ca_{2-x}Sr_xRuO_4$,[12,13] and vanadates like V_2O_3,[14,15] exhibit strong correlated multi-orbital characteristics. In these systems, the complex interplay between charge, spin, and orbital degrees of freedom gives rise to exotic quantum phenomena such as orbital-selective Mott transitions (OSMT)[16–19] and Hund metal behavior.[20–23]

Inter-orbital hybridization is an intrinsic quantum phenomenon in multi-orbital systems, manifesting in two forms: inter-site (between orbitals of neighboring atoms)[24–26] and on-site (between orbitals of the same atom).[27,28] Inter-site inter-orbital hybridization has been extensively studied; for example, it enhances superconducting pairing in materials such as iron-based superconductors[29] and the newly discovered $La_3Ni_2O_7$,[30] and it also disrupts the OSMT.[31–34] However, the investigations of on-site inter-orbital hybridization remain limited. The on-site inter-orbital hybridization, which is denoted as t', can also significantly affect the system properties, such as suppressing OSMT[17,35] and modifying the pseudogap behavior.[36] Notably, a systematic investigation of how t' modulates correlation strength of a system across various doping concentrations is lacking. Understanding this fundamental regulatory mechanism is essential for manipulating the correlation strength in doped multi-orbital systems.

To investigate a multi-orbital correlated system incorporating on-site inter-orbital hybridization t', we adopt the dynamical mean-field theory (DMFT).[37–39] In contrast to traditional mean-field approaches, DMFT accounts for full quantum dynamical fluctuations. It maps the original lattice model (Eq. (1)) onto an impurity Anderson model (Eq. (4)), which can be solved using numerical methods such as numerical renormalization group (NRG),[40] continuous-time quantum Monte Carlo (CT-QMC),[41] and exact diagonalization (ED).[42–44] The DMFT with NRG solver provides real-frequency spectra for single-orbital systems but faces challenges in multi-orbital cases with complex interactions. The DMFT with CT-QMC method numerically provides exact finite-temperature solutions for larger systems. However, it suffers from a sign problem when off-diagonal elements exist in the Green's function, along with high computational costs at low temperatures and the need for analytical continuation. ED solver (including the Lanczos method) is limited by the Hilbert space dimension for small impurity clusters. Finite bath discretization often yields spectral functions with discrete peaks. We employ the Lanczos exact diagonalization method as the impurity solver for three reasons: (i) For the two-orbital Anderson impurity model studied here, the Hilbert space dimension remains computationally feasible for the Lanczos method. (ii) Unlike the CT-QMC solver, Lanczos inherently avoids the sign problem caused by off-diagonal elements in Green's function resulting from inter-orbital hybridization. (iii) It enables direct computation of the real-frequency Green's function after DMFT convergence, enabling direct comparison with experimental spectra.

[†]Corresponding author. E-mail: sunjian@sspu.edu.cn

© 2026 Chinese Physical Society and IOP Publishing Ltd. All rights, including for text and data mining, AI training, and similar technologies, are reserved.

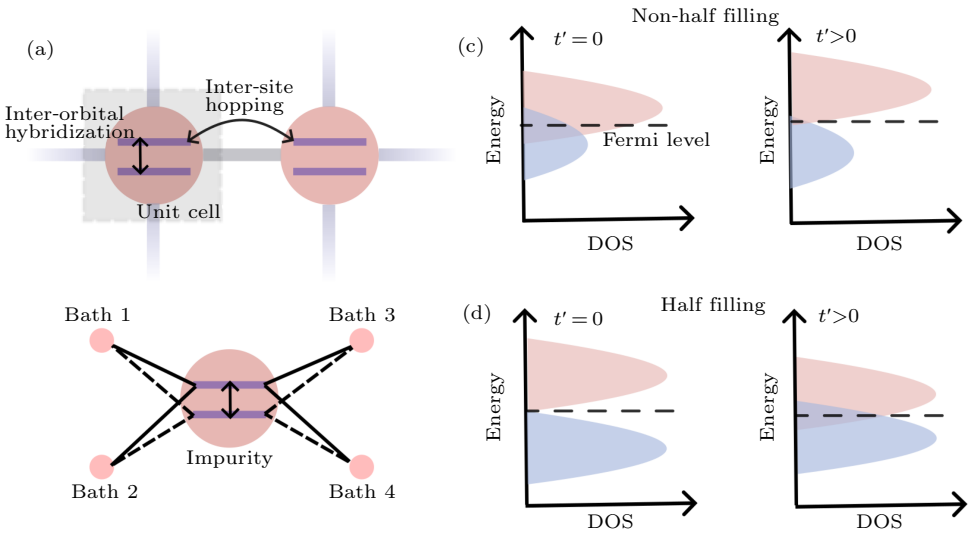


Fig. 1. (a) Schematic representation of a two-orbital square lattice. (b) Schematic illustration of a shared-bath type impurity Anderson model with four bath sites. Solid and dashed lines represent the hybridization between the bath sites and the two impurity orbitals, respectively. Panels (c) and (d) are schematic depictions of the influence of inter-orbital hybridization on the correlation strength of the system under same electron correlation interaction. The system is in a non-half-filling state in panel (c) and half-filling state in panel (d). (c) In the non-half-filling scenario, the introduction of t' causes a decrease in the density of state near the Fermi surface, leading to an increase in the system's correlation strength. (d) In the half-filling scenario, in contrast to panel (c), the system is in an insulating state when $t'=0$.

In this study, we investigate the effect of on-site inter-orbital hybridization t' on the correlation strength of the system. Using the DMFT method, a two-orbital correlated model with equal bandwidths at various occupation levels is examined. Notably, t' exhibits opposite effects on the correlation strength in the half-filled and non-half-filled systems. Figures 1(c) and 1(d) schematically illustrate these conclusions. Here, the red and blue regions represent the density of states (DOS) for the upper and lower Hubbard bands, respectively and the dashed line indicates the Fermi level. The correlation strength is quantified using the spectral weight overlap between the Hubbard bands at the Fermi level, where a larger overlap corresponds to a weaker correlation strength. Figure 1(c) depicts a non-half-filled system, whereas figure 1(d) corresponds to the half-filled case; the left panels show the results for $t'=0$, and the right panels show those for $t'>0$. As shown in Fig. 1(c), vanishing t' increases the spectral overlap, indicating weakened correlations. Conversely, in the half-filled system (Fig. 1(d)), the nonzero t' increases the spectral overlap, signifying weakened correlations.

2. Model and methodology

Layered perovskite ruthenates, particularly Sr_2RuO_4, provide direct physical motivation for the proposed model.[12,28] In undoped Sr_2RuO_4, the near-ideal square-lattice symmetry forbids direct hybridization between different t_{2g} orbitals on the same Ru site. However, lattice distortions induced by external perturbations can disrupt this symmetry. A prototypical example is $Ca_{2-x}Sr_xRuO_4$: substituting smaller Ca^{2+} ions for larger Sr^{2+} ions causes tilting and rotation of the RuO_6 octahedra. This distortion reduces the local symmetry and activates a finite on-site hybridization t' between the formerly orthogonal orbitals. Motivated by this universal mechanism, in which broken symmetry enables significant on-site inter-orbital hybridization, we employ a minimal two-orbital Hubbard model (Fig. 1(a)) to investigate how t' modulates electronic correlations across the doping levels within strong interaction regimes. By focusing on the interplay of t', on-site electron–electron interaction U, and doping level n, our model transcends material-specific details to reveal the fundamental principles governing correlation strength in multi-orbital systems. The model Hamiltonian is defined as follows:

$$H = H_0 + H_{\rm I}, \tag{1}$$

where H_0 is the non-interaction part,

$$\begin{aligned} H_0 = & -t\sum_{\langle ij\rangle}\sum_{l\sigma}(c^{\dagger}_{il\sigma}c_{jl\sigma}+c^{\dagger}_{jl\sigma}c_{il\sigma})-\mu\sum_{il\sigma}c^{\dagger}_{il\sigma}c_{il\sigma} \\ & -t'\sum_{i,l<l'\sigma}(c^{\dagger}_{il\sigma}c_{il'\sigma}+c^{\dagger}_{il'\sigma}c_{il\sigma}), \end{aligned} \tag{2}$$

$H_{\rm I}$ is the interaction part, which includes all Hund's coupling terms,

$$\begin{aligned} H_{\rm I} = & U\sum_{il}n_{il\uparrow}n_{il\downarrow}+U'\sum_{i,l<l'}n_{il\uparrow}n_{il'\downarrow} \\ & +(U'-J)\sum_{i,l<l',\sigma}n_{il\sigma}n_{il'\sigma} \\ & -J\sum_{i,l\neq l'}c^{\dagger}_{il\uparrow}c_{il\downarrow}c^{\dagger}_{il'\downarrow}c_{il'\uparrow}+J\sum_{i,l\neq l'}c^{\dagger}_{il\uparrow}c^{\dagger}_{il\downarrow}c_{il'\downarrow}c_{il'\uparrow}. \end{aligned} \tag{3}$$

Operator $c^{\dagger}_{il\sigma}$ (or $c_{il\sigma}$) creates (or annihilates) an electron with spin σ in orbital l at site i. Throughout this study, the inter-site hopping amplitude t within the same orbital is used as the energy unit. On-site inter-orbital hybridization is represented by t', where μ is the chemical potential. The on-site electron correlation strength within the same orbital is U, where U'

denotes the inter-orbital electron correlation strength. Hund's coupling is represented by J, with $J/U = 0.25$,[21] and $U = U' + 2J$ to ensure rotation invariance.[14,21]

The DMFT method is used to study the multi-orbital Hubbard model Eq. (1). DMFT maps the original lattice model Eq. (1), which has higher degrees of freedom, onto an equivalent impurity Anderson model with lower degrees of freedom. The impurity Anderson model is expressed as follows:

$$\begin{aligned} H_{\text{imp}} =& \sum_{k\sigma} \varepsilon_{k\sigma} a^{\dagger}_{k\sigma} a_{k\sigma} + \sum_{kl\sigma} V_{kl\sigma} (a^{\dagger}_{k\sigma} d_{l\sigma} + d^{\dagger}_{l\sigma} a_{k\sigma}) \\ & - t' \sum_{l<l'\sigma} (d^{\dagger}_{l\sigma} d_{l'\sigma} + d^{\dagger}_{l'\sigma} d_{l\sigma}) - \mu \sum_{l\sigma} d^{\dagger}_{l\sigma} d_{l\sigma} \\ & + U \sum_{l} n_{l\uparrow} n_{l\downarrow} + U' \sum_{l<l'} n_{l\uparrow} n_{l'\downarrow} \\ & + (U' - J) \sum_{l<l',\sigma} n_{l\sigma} n_{l'\sigma} \\ & - J \sum_{l\neq l'} d^{\dagger}_{l\uparrow} d_{l\downarrow} d^{\dagger}_{l'\downarrow} d_{l'\uparrow} + J \sum_{l\neq l'} d^{\dagger}_{l\uparrow} d^{\dagger}_{l\downarrow} d_{l'\downarrow} d_{l'\uparrow}. \end{aligned} \tag{4}$$

Here, the operator $a^{\dagger}_{k\sigma}$ ($a_{k\sigma}$) represents the creation (annihilation) of an electron with spin σ at the k-th bath site. The operator $d^{\dagger}_{k\sigma}$ ($d_{k\sigma}$) denotes the creation (annihilation) of an electron with spin σ in the l-th orbital of the impurity site. The parameter $\varepsilon_{k\sigma}$ represents the kinetic energy of an electron with spin σ at the k-th bath site. The electron coupling strength between the l-th orbital at the impurity site and the k-th bath site is denoted by $V_{kl\sigma}$. Parameters t', μ, U, U', J of the impurity Anderson model have the same physical meaning as those of the lattice model given by Eq. (1). Notably, $\varepsilon_{k\sigma}$ and $V_{kl\sigma}$ are self-consistent parameters obtained through the DMFT procedure.

Subsequently, the impurity Anderson model Eq. (4) can be solved accurately using numerical or theoretical methods. The results of the original lattice model are obtained using a self-consistent procedure. In this study, the Lanczos exact diagonalization method is used as an impurity solver. Green's function includes off-diagonal terms owing to hybridization between different orbitals. Therefore, we adopt a shared-bath site configuration,[38] in which all impurity orbitals share the same set of bath sites. As shown in Fig. 1(b), this configurations involves four shared-bath sites. In our study, the correlated impurity site of the Anderson model has 2 orbitals hybridized with 9 shared bath sites. Therefore, the number of sites in this model is 11. This approach not only simplifies the calculation of off-diagonal terms but also enables an increased number of baths without increasing the computational demands, thereby enhancing the accuracy of the results.

The zero-temperature Green's function is given by[45]

$$\begin{aligned} G_{mm}(\omega) &= G^{(+)}_{mm}(\omega) + G^{(-)}_{mm}(\omega) \\ &= \langle \phi_0 | c_m \frac{1}{\omega - E_0 + H + \mathrm{i}\eta} c^{\dagger}_m | \phi_0 \rangle \\ &\quad + \langle \phi_0 | c^{\dagger}_m \frac{1}{\omega + E_0 - H + \mathrm{i}\eta} c_m | \phi_0 \rangle. \end{aligned} \tag{5}$$

Here, $|\phi_0\rangle$ is the ground state of the system, obtained by directly running the Lanczos method. To demonstrate the application of the Lanczos method to calculate the Green's function,[43] we take $G^{(+)}_{mm}(\omega) = \langle \phi_0 | c_m \frac{1}{\omega - E_0 + H + \mathrm{i}\eta} c^{\dagger}_m | \phi_0 \rangle$ as an example. We initiate the Lanczos recursion with the state $|\psi_0\rangle = c^{\dagger}_m |\phi_0\rangle$ and apply the recurrence relation: $|\psi_{n+1}\rangle = H|\psi_n\rangle - a^{(+)}_n |\psi_n\rangle - (b^{(+)}_n)^2 |\psi_{n-1}\rangle$, where $a^{(+)}_n = \frac{\langle \psi_n | H | \psi_n \rangle}{\langle \psi_n | \psi_n \rangle}$ and $(b^{(+)}_n)^2 = \frac{\langle \psi_n | \psi_n \rangle}{\langle \psi_{n-1} | \psi_{n-1} \rangle}$. This recursion constructs an orthogonal basis spanning the Krylov subspace. In this basis, Hamiltonian such as equation (4) is represented by a tridiagonal matrix, where $\{a^{(+)}_n\}$ are the diagonal elements and $\{b^{(+)}_n\}$ are the off-diagonal elements. Thus, the resolvent matrix element reduces to a continued fraction as follows:

$$G^{(+)}_{mm}(\omega) = \cfrac{\langle \phi_0 | c_m c^{\dagger}_m | \phi_0 \rangle}{\omega - a^{(+)}_0 - \cfrac{b^{(+)2}_1}{\omega - a^{(+)}_1 - \cfrac{b^{(+)2}_2}{\omega - a^{(+)}_2 - \ldots}}}. \tag{6}$$

The procedure for $G^{(-)}_{mm}(\omega)$ is identical but starts with the state $c_m|\phi_0\rangle$, yielding a continued fraction with coefficients $\{a^{(-)}_n\}$ and $\{b^{(-)}_n\}$.

Thus, the total Green's function obtained via the Lanczos method is

$$\begin{aligned} G_{mm}(\omega) &= G^{(+)}_{mm}(\omega) + G^{(-)}_{mm}(\omega) \\ &= \cfrac{\langle \phi_0 | c_m c^{\dagger}_m | \phi_0 \rangle}{\omega - a^{(+)}_0 - \cfrac{b^{(+)2}_1}{\omega - a^{(+)}_1 - \cfrac{b^{(+)2}_2}{\omega - a^{(+)}_2 - \ldots}}} \\ &\quad + \cfrac{\langle \phi_0 | c^{\dagger}_m c_m | \phi_0 \rangle}{\omega + a^{(-)}_0 - \cfrac{b^{(-)2}_1}{\omega + a^{(-)}_1 - \cfrac{b^{(-)2}_2}{\omega + a^{(-)}_2 - \ldots}}}. \end{aligned} \tag{7}$$

The inclusion of inter-orbital hybridization terms leads to the appearance of off-diagonal elements in Green's function. The matrix form of this Green's function is given below:

$$G(\omega) = \begin{pmatrix} G_{mm}(\omega), & G_{mn}(\omega) \\ G_{nm}(\omega), & G_{nn}(\omega) \end{pmatrix}. \tag{8}$$

Let m and n denote the states in orbital 1 and orbital 2 with spin σ, respectively. The off-diagonal terms of the Green's function prevent the direct application of the Lanczos method. To solve this problem, we introduce two new operators $c_f = c_m + c_n$, $c_k = c_m + \mathrm{i}c_n$, along with their conjugates. The Green's function of these two operators are

$$\begin{aligned} G_{ff} &= G_{mm} + G_{nn} + G_{mn} + G_{nm}, \\ G_{kk} &= G_{mm} + G_{nn} - \mathrm{i}G_{mn} + \mathrm{i}G_{nm}. \end{aligned} \tag{9}$$

Here, G_{ff} and G_{kk} are the Green's function of operators c_f, $c^{\dagger}_f$, and c_k, $c^{\dagger}_k$, respectively. They are defined by expressions similiar to those in Eq. (7). Subsequently, the off-diagonal Green's

function G_{mn} and G_{nm} can be represented as linear combinations of the diagonal Green's function G_{ff} and G_{kk},

$$\begin{aligned} G_{mn} &= \frac{1}{2}[G_{ff} + \mathrm{i}G_{kk} - (1+\mathrm{i})(G_{mm}+G_{nn})], \\ G_{nm} &= \frac{1}{2}[G_{ff} - \mathrm{i}G_{kk} - (1-\mathrm{i})(G_{mm}+G_{nn})]. \end{aligned} \tag{10}$$

The full dynamical mean field self-consistent procedure comprises the following steps:

(i) Initialize the impurity Anderson model Hamiltonian (Eq. (4)) with the initial parameters: bath energy $\{\varepsilon_{k\sigma}\}$ and bath-impurity hybridization $\{V_{kl\sigma}\}$. Calculate the full Green's function matrix $G_{\mathrm{imp}}(\mathrm{i}\omega_n)$ using the Lanczos method mentioned above. It should be noted that the choice of initial parameters has a substantial influence on self-consistent convergence. Through multiple tests, we find that the determination of initial parameters can commence from the half-filling case. The initial parameters should make the density of states of the impurity Anderson model Eq. (4) symmetric about the chemical potential. Under such circumstances, more favorable convergence results can be achieved. For non-half-filled systems, the parameters self-consistently obtained in the half-filled case can serve as the initial parameters.

(ii) Calculate the Weiss Green's function of the impurity Anderson model,

$$g^0_{\mathrm{imp}}(\mathrm{i}\omega_n) = \frac{1}{\mathrm{i}\omega_n \hat{I} - H^0_{\mathrm{imp}}}, \tag{11}$$

where H^0_{imp} denotes the non-interaction impurity Anderson model (where U, U', and J are set to zero), and $\hat{I}$ is the identity matrix that has the same dimension as the Green's function matrix of impurity Anderson model (Eq. (8)).

(iii) Calculate the self-energy using Dyson equation

$$\Sigma(\mathrm{i}\omega_n) = [g^0_{\mathrm{imp}}(\mathrm{i}\omega_n)]^{-1} - G^{-1}_{\mathrm{imp}}(\mathrm{i}\omega_n). \tag{12}$$

(iv) Calculate the lattice Green's function

$$G_{\mathrm{lat}}(\mathrm{i}\omega_n) = \frac{1}{N}\sum_n \frac{1}{\mathrm{i}\omega\hat{I} + H_0(k) - \Sigma(\mathrm{i}\omega_n)}, \tag{13}$$

where $H_0(k)$ is the non-interaction lattice model Hamiltonian (Eq. (2)).

(v) Calculate the Weiss Green's function of the lattice model (Eq. (1)),

$$[g^0_{\mathrm{lat}}(\mathrm{i}\omega_n)]^{-1} = [G_{\mathrm{lat}}(\mathrm{i}\omega_n)]^{-1} + \Sigma(\mathrm{i}\omega_n). \tag{14}$$

(vi) Employ the conjugate gradient method to minimize the difference between $g^0_{\mathrm{lat}}(\mathrm{i}\omega_n)$ and $g^0_{\mathrm{imp}}(\mathrm{i}\omega_n)$, defined as[38]

$$d = \frac{1}{\omega_n}\sum_n \|g^0_{\mathrm{lat}}(\mathrm{i}\omega_n) - g^0_{\mathrm{imp}}(\mathrm{i}\omega_n)\|^2, \tag{15}$$

to determine new sets of parameters $\{\varepsilon_{k\sigma}\}$ and $\{V_{kl\sigma}\}$ for the impurity Anderson model Hamiltonian Eq. (4).

Iterate steps (ii)–(vi) until convergence is achieved, where convergence is defined as the maximum absolute difference in the local lattice Green's function $G_{\mathrm{lat}}(\mathrm{i}\omega_n)$ between two consecutive self-consistent loops is smaller than a predefined threshold: $\delta/t = \max\left|G^{(m)}_{\mathrm{lat}}(\mathrm{i}\omega_n) - G^{(m-1)}_{\mathrm{lat}}(\mathrm{i}\omega_n)\right| < 10^{-4}$, where m indexes the iteration number. Subsequently, the Green's function of the original lattice Eq. (1) is obtained through a self-consistent equation.

In our calculation, a self-consistent procedure is performed on a mesh of Matsubara frequencies $\omega_n = (2n+1)\pi/\beta$. Here, $\beta t = 200$ and the spectral function is broadened to $\eta/t = 0.05$. In our program, by adopting a sparse matrix representation of the impurity Anderson model Hamiltonian Eq. (4), significant memory savings are achieved. This enables the program to be executed on a single core. Each DMFT loop requires approximately 70 min per core. Consequently, it is feasible to complete computations on a small workstation, which results in substantial savings in computational resources. The results shown in Fig. 2 are calculated using a small workstation. The phase diagram shown in Fig. 3 is obtained using the Magic Cube III at the Shanghai Supercomputer Center.

3. Results

In single-band systems, the electron correlation strength mainly originates from the electron–electron Coulomb interactions. However, in multi-orbital systems, the correlation stems not only from the Coulomb interactions between the electrons in the same or different orbitals but also from Hund's coupling. All these factors increase the correlation strength of the system, resulting in an increase in the effective mass m^* of the quasi-particles. The relationship between the effective mass and the quasi-particle weight Z is given by $m^*/m = 1/Z = 1 - \frac{\partial}{\partial\omega}\mathrm{Re}\Sigma(\omega + \mathrm{i}0^+)|_{\omega=0}$.[37] Therefore, in this study, we use a quasi-particle weight Z to represent the correlation strength of the system.

To explore the effect of the on-site inter-orbital hybridization strength t' on the correlation strength, first, a quarter-filled ($n = 1.0$) scenario is examined. Figure 2(a) shows the quasi-particle weight Z as a function of the Coulomb interaction strength U/t for different values of t'. The observed decline in Z with increasing t' indicates an increase in the correlation strength. Figure 2(b) shows the DOS as a function of t' at $U/t = 4.0$. The suppression of the DOS near the Fermi energy ($(\omega - \mu)/t = 0$) upon increasing t' reduces the spectral weight overlap between the Hubbard bands. This spectral decoherence directly indicates an enhancement in the correlation strength of the system. Figure 2(c) presents the imaginary part of the self-energy as a function of the Matsubara frequency. The reduction in the imaginary part of the self-energy as ω approaches zero with increasing t' further supports the

conclusion of enhanced correlation strength. In summary, at quarter-filling, increasing the inter-orbital hybridization t' enhances the system's correlation.

In the half-filling case ($n = 2.0$), the results exhibite an inverse relationship to those in the quarter-filling case. Figure 2(d) shows the variation of Z with U/t under different t' conditions. An increase in t' leads to an increase in the quasi-particle weight, indicating a weakening of the correlation strength at half-filling. This implies that under half-filling conditions, the correlation strength of the system decreases as t' increases. At half-filling, figure 2(e) shows the DOS and figure 2(f) shows the imaginary part of the self-energy. As shown in Fig. 2(e), the DOS for different values of t' exhibits a gap at the Fermi level. Because of the finite number of bath sites, the DOS displays several peaks. The presence of a gap in the DOS at the Fermi surface does not necessarily indicate a Mott metal–insulator transition. Therefore, the imaginary part of the Matsubara frequency self-energy is analyzed. Figure 2(f) reveals that the imaginary part of the self-energy diverges at $t' = 0$, which is a characteristic of the Mott metal–insulator transition. In contrast, for non-zero t', the system remains in a metallic state. Notably, the imaginary part of the self-energy is smaller at $t'/t = 0.2$ than at $t'/t = 0.4$, further supporting the weakening of the correlation as t' increases. This is in contrast to the quarter-filling results, where the correlation strength increases with t', highlighting the opposing influence of inter-orbital hybridization on the correlation strength at different doping levels. At half-filling, when t' is present, as shown in Fig. 2(d), the quasi-particle weight Z remains low and forms a plateau over a wide range of U values. While reminiscent of Hund metal behavior, the underlying mechanisms are fundamentally distinct. In Hund metal, this plateau occurs at non-half-filling regime. Hund's coupling J promotes high-spin configurations by aligning electron spins parallel across orbitals, and suppresses orbital fluctuations, then increases the electron effective mass m^*, thereby reducing the quasi-particle weight Z. Electron distribution across orbitals weakens Coulomb interactions, raising the critical U_c for the metal–insulator transition and stabilizing the plateau. In the system with t', the plateau develops specifically at half-filling. In contrast to a metal–insulator transition in the system without t', the electron motion t' between orbitals reduces localization. Strong interactions simultaneously lower the quasi-particle weight Z and create a Hund-metal-like plateau.

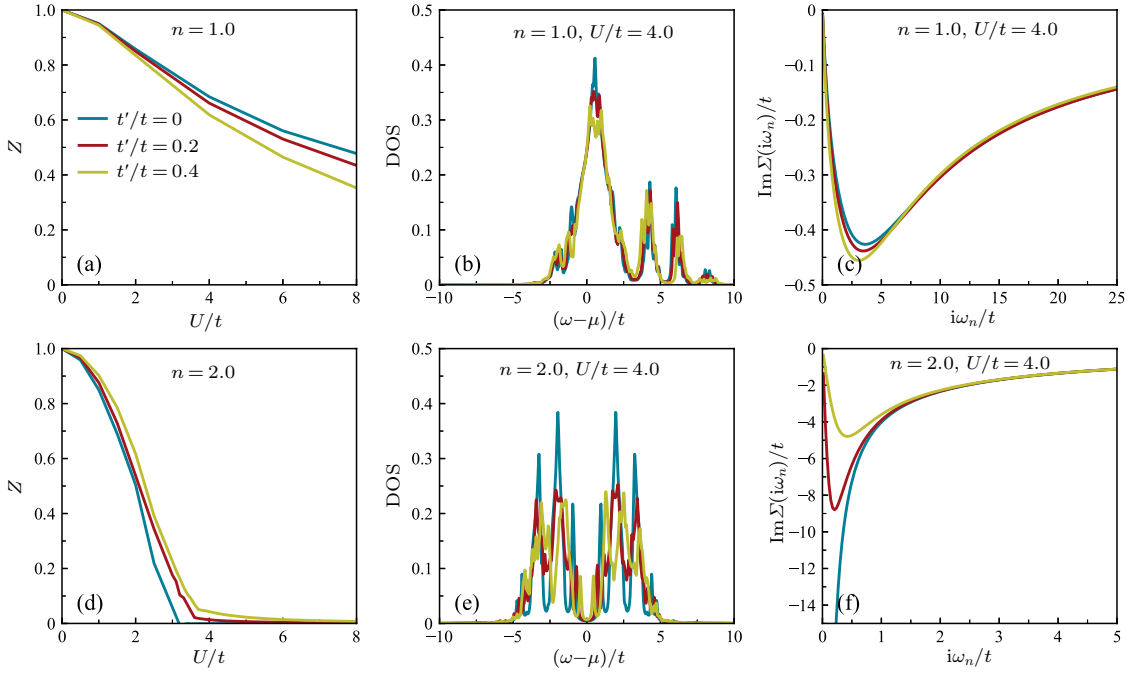


Fig. 2. (a) At quarter-filling, the quasi-particle weight varies as the Coulomb interaction U/t. The blue, red, and yellow lines represent the results obtained with inter-orbital hybridization $t'/t = 0.0$, $t'/t = 0.2$, and $t'/t = 0.4$, respectively. (b) The density of states (DOS) at quarter-filling and $U/t = 4.0$. (c) The imaginary part of the self-energy at quarter-filling and $U/t = 4.0$. (d) At half-filling, the quasi-particle weight varies as a function of the interaction U/t. (e) The density fo states (DOS) at half-filling and $U/t = 4.0$. (f) The imaginary part of self-energy at half-filling and $U/t = 4.0$.

In the following study, we systematically explore the relationship between the correlation strength and the on-site inter-orbital hybridization at various doping levels. Figures 3(a)–3(i) depict the quasi-particle weight as a function of the electron interaction U/t for different fillings. The effects of inter-orbital hybridization on the quasi-particle weight at both half-filling and non-half-filling are consistent with our findings in the quarter-filling and half-filling scenarios. Figure 3(j) shows the variation in the difference in the quasi-particle weight between $t'/t = 0.2$ and $t'/t = 0.0$ as a function of the filling at $U/t = 4.0$. At near half-filling ($1.75 < n < 2.25$), the quasi-particle weight corresponding to $t'/t = 0.2$ is higher, indicat-

ing that the correlation strength decreases as t' increases. Conversely, figures 3(d)–3(f) show that for $t'/t \neq 0$, the quasi-particle weight remains low over a wide range of U/t, and there is no metal–insulator transition, exhibiting Hund's metal behavior. From Fig. 3(j) for $n < 1.75$ and $n > 2.25$ and Fig. 3(k) for $n < 1.80$ and $n > 2.20$, an increase in t' is associated with a decrease in quasi-particle weight and an increase in correlation length.

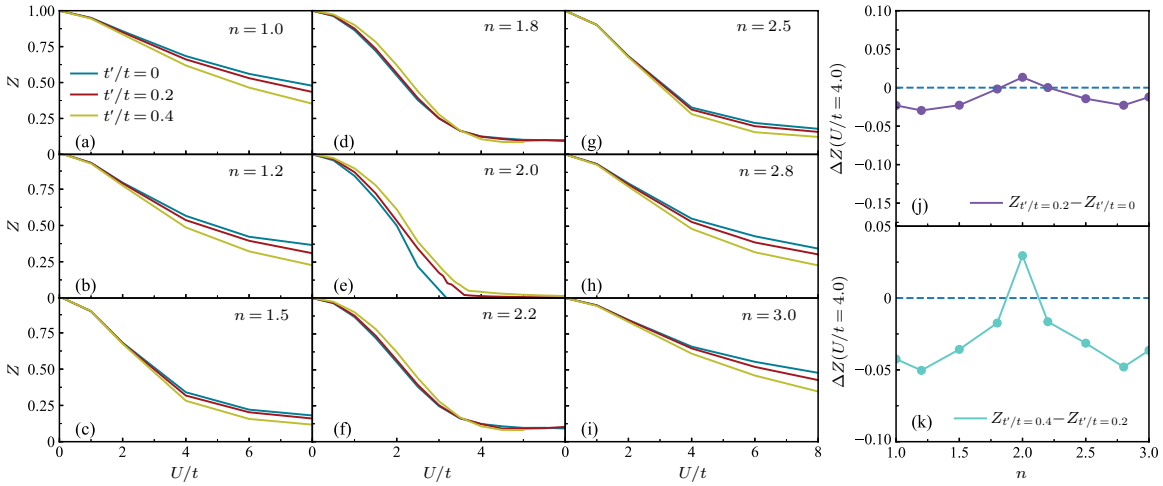


Fig. 3. (a)–(i) The variation of the quasi-particle weight with the interaction strength U/t. The blue, red, and yellow lines represent the results obtained with inter-orbital hybridization $t'/t = 0.0$, $t'/t = 0.2$, and $t'/t = 0.4$, respectively, at different occupation levels. Panel (j) represents the difference in the quasi-particle weight at $U/t = 4.0$ between $t'/t = 0.2$ and $t'/t = 0.0$. Panel (k) represents the difference in the quasi-particle weight at $U/t = 4.0$ between $t'/t = 0.4$ and $t'/t = 0.2$.

To emphasize the effects of the on-site inter-orbital hybridization t', we use a two-orbital Hubbard model with equal bandwidths to eliminate the influence of different bandwidths. In this degenerate model, t' is equivalent to the crystal field splitting energy Δ_c, becasue upon diagonalization, t' contributes to the diagonal elements and effectively acts as Δ_c. The interaction terms retain the same form as in the original model. At quarter-filling, Manini *et al.* found that Δ_c enhanced the correlation strength of the system,[46] and at half-filling, Werner *et al.* found that Δ_c weakened the correlation strength,[20] and our results are consistent with their findings.

When the orbital widths of the system are no longer identical, the effects of inter-orbital hybridization t' and the crystal field splitting energy Δ_c become inequivalent. This is because, upon diagonalizing the non-interaction part in the new atomic orbital space, the form of the interaction part becomes rather complex, and numerous new forms of interactions occur. At this stage, the model is no longer equivalent to that of the crystal-field splitting energy. Next, we check whether the model with different orbital bandwidths gives the same conclusions as the earlier model with varying doping and t'.

Without loss of generality, we adopt a model with an orbital-width ratio of 2:1 as follows:

$$
\begin{aligned}
H = & -\sum_{\langle ij\rangle}\sum_{l\sigma} t_l (c^{\dagger}_{il\sigma} c_{jl\sigma} + c^{\dagger}_{jl\sigma} c_{il\sigma}) \\
& - \mu \sum_{il\sigma} c^{\dagger}_{il\sigma} c_{il\sigma} - t' \sum_{i,l<l'\sigma} (c^{\dagger}_{il\sigma} c_{il'\sigma} + c^{\dagger}_{il'\sigma} c_{il\sigma}) \\
& + U \sum_{il} n_{il\uparrow} n_{il\downarrow} + U' \sum_{i,l<l'} n_{il\uparrow} n_{il'\downarrow} \\
& + (U' - J) \sum_{i,l<l',\sigma} n_{il\sigma} n_{il'\sigma} \\
& - J \sum_{i,l\neq l'} c^{\dagger}_{il\uparrow} c_{il\downarrow} c^{\dagger}_{il'\downarrow} c_{il'\uparrow} + J \sum_{i,l\neq l'} c^{\dagger}_{il\uparrow} c^{\dagger}_{il\downarrow} c_{il'\downarrow} c_{il'\uparrow}. \qquad (16)
\end{aligned}
$$

In this model Eq. (16), the widths of the wide and narrow orbitals are $t_2 = t$ and $t_1 = t/2$, respectively. The interaction part of this model has the same form as that of the Hubbard model Eq. (3). Here, two occupation scenarios are calculated: half-filling ($n = 2.0$) and quarter-filling ($n = 1.0$). The quasi-particle weight is used here to characterize the correlation strength of the system, and the results are shown in Fig. 4.

In Fig. 4, the upper panel shows the quarter-filling case ($n = 1.0$). In this panel, sub-panels (a) and (b) show the quasi-particle weights Z_2 and Z_1 of the wide and narrow bands, respectively. As t'/t increases, both Z_2 and Z_1 of the wide and narrow bands decrease, indicating an enhancement in the correlation strength of the system. Conversely, the lower sub-panels (c) and (d) correspond to the half-filling case ($n = 2.0$) and show that both Z_2 and Z_1 increase as t'/t increases, which corresponds to a decrease in the correlation strength. These observations suggest that the influence of inter-orbital hybridization on the correlation strength of the system is a general mechanism applicable to both degenerate and non-degenerate band scenarios and does not stem from the crystal field splitting energy Δ_c. Moreover, models featuring different orbital widths are more representative of real materials.

Consequently, our findings indicate that on-site inter-orbital hybridization has opposite effects on the behavior of the system at different electron doping levels: (i) At half-filling, the correlation strength of the system is weakened,

thereby extending the range of electron interaction within which bad metallic behavior persists. (ii) Conversely, away from half-filling, an increase in the inter-orbital hybridization enhances the correlation strength. Thus, on-site inter-orbital hybridization exhibits a Janus-like (dual) influence, suppressing correlations at half-filling while strengthening them away from it.

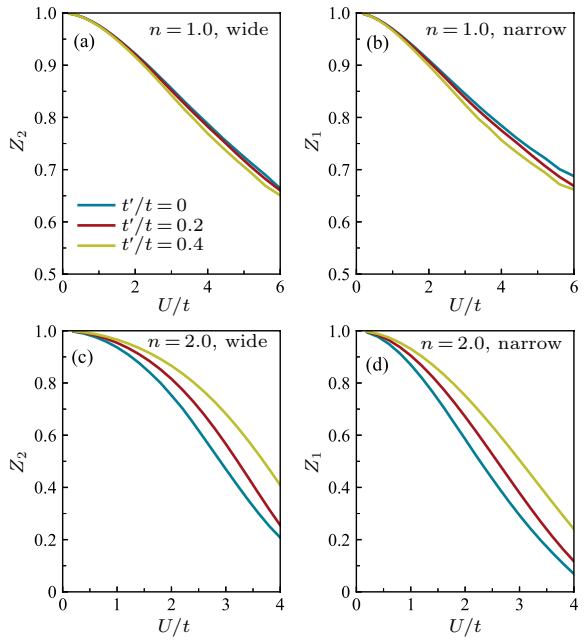


Fig. 4. Quasi-particle weight in the non-degenerate two-orbital Hubbard model: Panels (a) and (c) represent the wide orbital; panels (b) and (d) represent narrow orbital. The upper panels correspond to quarter filling ($n=1.0$), and the lower panels correspond to half-filling ($n=2.0$). The blue, red and yellow lines represent $t'/t_2=0.0$, $t'/t_2=0.2$ and $t'/t_2=0.4$, respectively.

To explain the effect of on-site inter-orbital hopping t' on the correlation strength, we use a two-orbital model in the atomic limit. In this limit, the distance between atoms is infinitely large, making inter-atomic electron hopping negligible. Consequently, only the on-site energies, such as the Coulomb interaction U between electrons, Hund's coupling J, and the inter-orbital hybridization t', influence the atomic levels. Within the atomic limit, the correlation strength can be indirectly characterized by the energy cost associated with changing the number of electrons in the system. The larger energy required to alter the electron number signifies a stronger correlation strength, and vice versa. The multi-orbital atomic Hamiltonian is expressed as follows:

$$\begin{aligned} H_{\text{atom}} = & -t'\sum_{l<l',\sigma}(c^{\dagger}_{l\sigma}c_{l'\sigma}+c^{\dagger}_{l'\sigma}c_{l\sigma})-\mu\sum_{l\sigma}c^{\dagger}_{l\sigma}c_{l\sigma} \\ & +U\sum_{l}n_{l\uparrow}n_{l\downarrow}+U'\sum_{l<l'}n_{l\uparrow}n_{l'\downarrow} \\ & +(U'-J)\sum_{l<l',\sigma}n_{l\sigma}n_{l'\sigma} \\ & -J\sum_{l\neq l'}c^{\dagger}_{l\uparrow}c_{l\downarrow}c^{\dagger}_{l'\downarrow}c_{l'\uparrow}+J\sum_{l\neq l'}c^{\dagger}_{l\uparrow}c^{\dagger}_{l\downarrow}c_{l'\downarrow}c_{l'\uparrow}. \end{aligned} \tag{17}$$

Here, the on-site inter-orbital hybridization t', Coulomb interaction U, Hund coupling J, and chemical potential μ have the same physical meaning as in the interaction part of Hubbard model Eq. (3). In this atomic limit, we set the energy unit $t=1.0$.

In the atomic limit, there are two fundamental processes for changing the number of electrons: (i) the addition of an electron, which requires additional energy $E_+=E_0(N+1)-E_0(N)$, and (ii) the removal of an electron, which requires removal energy $E_-=E_0(N)-E_0(N-1)$. The correlation strength of the system is then characterized by the larger value of these two energy costs, denoted as $\Delta=\max(E_+,E_-)$.

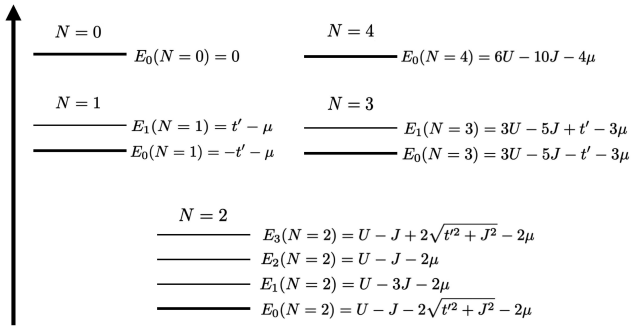


Fig. 5. The energy levels of atomic limit vary across different occupancy scenarios. The bolded lines represent ground state energy for certain occupancies.

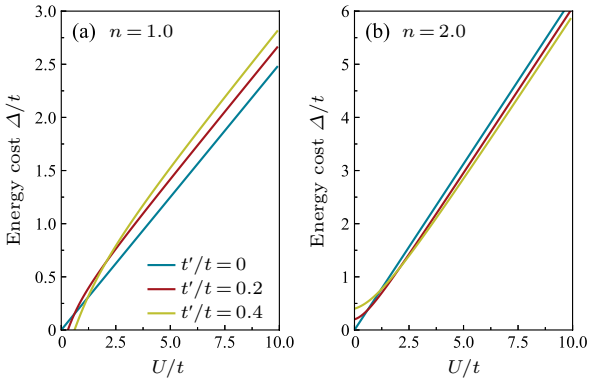


Fig. 6. Panels (a) and (b) show the energy cost *versus* electron interaction U/t for a single-electron change at quarter-filling ($n=1.0$) and half-filling ($n=2.0$), respectively. On-site interorbital hybridizations are indicated by $t'/t=0.0$ (blue), 0.2 (red), and 0.4 (yellow).

Specifically, the maximum energy cost Δ for changing the electron number is analyzed for two cases: quarter-filling ($N=1$) and half-filling ($N=2$). (i) Quarter-filling ($N=1$): Using the atomic energy levels shown in Fig. 5, the additional energy required to add an electron is $E_+=E_0(N=2)-E_0(N=1)=U-J-2\sqrt{t'^2+J^2}+t'-\mu$. The energy required to remove an electron is $E_-=E_0(N=1)-E_0(N=0)=-t'+\mu$. Consequently, the correlation strength can be expressed as $\Delta/t=\max(E_+,E_-)$. For a system with occupation number $N=1$, we define the system energy at $N=0$ occupation as the chemical potential μ, where $\mu=0$. Figure 6(a) shows the variation of Δ/t with U/t for $t'/t=0$, 0.2, 0.4. In the range of large values of U/t, Δ/t increases as t'/t increases, indicating that the correlation strength of the system increases with

increasing t'. (ii) Half-filling ($N = 2$): Here, the system possesses electron–hole symmetry. The energy required to add an electron (E_+) is identical to that required to remove an electron (E_-). Therefore, the correlation strength can be expressed as $\Delta/t = E_+ = E_- = 2U - 4J - t' + 2\sqrt{t'^2 + J^2} - \mu$. Owing to this symmetry, the chemical potential is $\mu = 3U/2 - 5J/2$. In Fig. 6(b), Δ/t is plotted as a function of U/t for $t'/t = 0.0, 0.2, 0.4$. It can be observed that in the larger U/t regime, Δ/t decreases as t'/t increases. This indicates that the correlation strength of the system decreases with increasing t'.

Through this single-atom model, we obtain trends consistent with those calculated using DMFT. This demonstrates that the strength of on-site inter-orbital hopping t' exerts opposite effects on the correlation strength of the system depending on the filling: weakening it at half-filling, but strengthening it at the non-half-filling.

4. Conclusions

Using dynamical mean-field theory, we systematically investigated the effect of on-site inter-orbital hybridization t' on correlation strength in a two-orbital Hubbard model on a square lattice. Our results reveal the Janus effect of t' on the correlation strength at different doping levels. At half-filling, increasing t' suppresses the correlation strength, maintaining a metallic state over a wide interaction U range, exhibiting low quasi-particle weight Z. Away from half-filling, increasing t' enhances the correlation strength, which is manifested by increased quasi-particle weight Z. Our findings provide a new interpretive framework for experimental observations of the filling-dependent correlation strength in multi-orbital systems and offer a potential perspective for analyzing how correlation strength and doping may influence superconductivity such as in $La_3Ni_2O_7$.

Acknowledgements

Project supported by the National Natural Science Foundation of China (Grant No. 12174327) and the Natural Science Foundation of Shandong Province, China (Grant No. ZR2023ZD09).

References

[1] Kamihara Y, Watanabe T, Hirano M and Hosono H 2008 *J. Am. Chem. Soc* **130** 3296
[2] Hsu T, Luo J, Yeh K, Chen T, Huang T, Wu P M, Lee Y, Huang Y, Chu Y, Yan D and Wu M 2008 *Proc. Natl. Acad. Sci. USA* **105** 14262
[3] Stewart G R 2011 *Rev. Mod. Phys.* **83** 1589
[4] Li J and Wang Y P 2008 *Chin. Phys. Lett.* **25** 2232
[5] Jiang Q, Kang Y T and Yao D X 2013 *Chin. Phys. B* **22** 087402
[6] Sun H, Huo M, Hu X, Li J, Liu Z, Han Y, Tang L, Mao Z, Yang P, Wang B, Cheng J, Yao D, Zhang G and Wang M 2023 *Nature* **621** 493
[7] Wang Y, Jiang K, Wang Z, Zhang F C and Hu J 2024 *Phys. Rev. B* **110** 205122
[8] Wang G, Wang N N, Shen X L, Hou J, Ma L, Shi L F, Ren Z A, Gu Y D, Ma H M, Yang P T, Liu Z Y, Guo H Z, Sun J P, Zhang G M, Calder S, Yan J Q, Wang B S, Uwatoko Y and Cheng J G 2024 *Phys. Rev. X* **14** 011040
[9] Zhang M, Zhang Y, Guo H and Yang F 2021 *Chin. Phys. B* **30** 108204
[10] Wang M, Wen H H, Wu T, Yao D X and Xiang T 2021 *Chin. Phys. Lett.* **41** 077402
[11] Jiang K, Wang Z and Zhang F C 2024 *Chin. Phys. Lett.* **41** 017402
[12] Nakatsuji S, Hall D, Balicas L, Fisk Z, Sugahara K, Yoshioka M and Maeno Y 2003 *Phys. Rev. Lett.* **90** 137202
[13] Anisimov V I, Nekrasov I A, Kondakov D E, Rice T M and Sigrist M 2002 *Eur. Phys. J. B* **25** 191
[14] Castellani C, Natoli C R and Ranninger J 1978 *Phys. Rev. B* **18** 4945
[15] Grieger D and Fabrizio M 2015 *Phys. Rev. B* **92** 075121
[16] Neupane M, Richard P, Pan Z H, Xu Y M, Jin R, Mandrus D, Dai X, Fang Z, Wang Z and Ding H 2009 *Phys. Rev. Lett.* **103** 097001
[17] Medici L d, Georges A and Biermann S 2005 *Phys. Rev. B* **72** 205124
[18] Song Y and Zou L J 2005 *Phys. Rev. B* **72** 085114
[19] Wang Y L, Huang L, Du L and Dai X 2005 *Chin. Phys. B* **25** 037103
[20] Werner P and Millis A J 2007 *Phys. Rev. Lett.* **99** 126405
[21] Georges A, de'Medici L and Mravlje J 2013 *Annu. Rev. Condens. Matter Phys.* **4** 137
[22] Stadler K M, Kotliar G, Weichselbaum A and Delft J V 2019 *Ann. Phys.* **405** 365
[23] De'Medici L, Mravlje J and Georges A 2011 *Phys. Rev. Lett.* **107** 256401
[24] Matt C E, Sutter D, Cook A M, *et al.* 2018 *Nat. Commun.* **9** 972
[25] Haule K and Kotliar G 2009 *New J. Phys.* **11** 025021
[26] Yu R, Zhu J X and Si Q M 2018 *Phys. Rev. Lett.* **121** 227003
[27] Kusunose H, Yotsuhashi S and Miyake K 2000 *Phys. Rev. B* **62** 4403
[28] Friedt O, Braden M, André G, Adelmann P, Nakatsuji S and Maeno Y 2001 *Phys. Rev. B* **63** 174432
[29] Stanescu T D, Galitski V and Das Sarma S 2008 *Phys. Rev. B* **78** 195114
[30] Qu X Z, Qu D W, Yi X W, Li W and Su G 2023 arXiv:2404.11369 [cond-mat]
[31] Kugler F B and Kotliar G 2022 *Phys. Rev. Lett.* **129** 096403
[32] Nunez-Fernandez Y and Hallberg K 2018 *J. Phys.: Conf. Ser.* **1041** 012002
[33] Yu R and Si Q M 2017 *Phys. Rev. B* **96** 125110
[34] Huang J, Yu R, Xu Z, *et al.* 2022 *Commun. Phys.* **5** 29
[35] Koga A, Kawakami N, Rice T M and Sigrist M 2005 *Phys. Rev. B* **72** 045128
[36] Winograd E A and de'Medici L 2014 *Phys. Rev. B* **89** 085127
[37] Georges A, Kotliar G, Krauth W and Rozenberg M J 1996 *Rev. Mod. Phys.* **68** 13
[38] Liebsch A and Ishida H 2011 *J. Phys.: Condens. Matter* **24** 053201
[39] Kotliar G, Savrasov S Y, Haule K, Oudovenko V S, Parcollet O and Marianetti C A 2006 *Rev. Mod. Phys.* **78** 865
[40] Bulla R, Costi T A and Pruschke T 2008 *Rev. Mod. Phys.* **80** 395
[41] Gull E, Millis A J, Lichtenstein A I, Rubtsov A N, Troyer M and Werner P 2011 *Rev. Mod. Phys.* **83** 349
[42] Caffarel M and Krauth W 1994 *Phys. Rev. Lett.* **72** 1545
[43] Dagotto E 1994 *Rev. Mod. Phys.* **66** 763
[44] Sun J, Liu Y and Song Y 2016 *Acta Phys. Sin.* **64** 247101 (in Chinese)
[45] Mahan G D 2000 *Many-Particle Physics*, 3nd edn. (New York: Springer) pp. 71–75
[46] Manini N, Santoro G E, Corso A D and Tosatti E 2002 *Phys. Rev. B* **66** 115107